ХИМИЯ РАСТИТЕЛЬНОГО СЫРЬЯ. 2023. №4. С. 325–334.
DOI: 10.14258/jcprm.20230412740

UDC 544.77.051

BIOSYNTHESIS, CHARACTERIZATION, ANTIMICROBIAL AND ANTICANCER PROPERTIES OF SILVER AND IRON NANOPARTICLES FROM *ROSA CANINA* L. EXTRACT

© ***A. Beyatli[1*], S. Shawuti[2], İ.A. Kariper[3], I.N. Korkut[2], Z. Aktaş[2], S.E. Kuruca[2]***

[1] University of Health Sciences, Selimiye Mah. Tıbbiye Cad., 38, Üsküdar/Istanbul, 34668 (Turkey), e-mail: ahmet.beyatli@sbu.edu.tr
[2] Istanbul University, Faculty of Medicine, Topkapı, Turgut Özal Millet Cd, Fatih/Istanbul, 34093 (Turkey)
[3] Erciyes University, Yenidoğan, Turhan Baytop Sokak, 1, Talas/Kayseri, 38280 (Turkey)

The goal of this research was to make Ag and Fe nanoparticles out of *Rosa canina* (RC) fruit extract and test their anticancer and antibacterial activity against human breast cancer cell line and different human pathogenic bacteria. Green synthesis used to synthesize silver (RC-AgNPs) and iron (RC-FeNPs) nanoparticles from the fruit aqueous extract of RC. The formation of nanoparticles was characterized by scanning electron microscopy with energy dispersive x-ray spectroscopy, UV-Vis and Fourier transform infrared (FTIR) spectroscopy. RC-AgNPs formation was also investigated the surface charge, particle size, and distribution using zetasizer analysis by DLS. Both nanoparticles showed different levels of cytotoxicity against AGS (human gastric adenocarcinoma) cell line, while RC-AgNPs was not cytotoxic to HUVEC (Human umbilical vein endothelial) cell line in same concentrations which expressing selective anticancer effect. RC-AgNPs showed antibacterial activity against multidrug pathogens, but RC-FeNPs failed to show such activity. The current study's findings point to the prospective applications of green synthesized RC-AgNPs and RC-FeNPs in the biomedical, pharmaceutical, and nanotechnology industries.

Keywords: *Rosa canina*; Green Synthesis, Ag-nanoparticle, Fe-nanoparticle, Anticancer, Antibacterial.

Introduction

Cancer is a disease that includes uncontrolled cell division and proliferation that can be due to the malfunction of molecular signals that control these events [1]. According to GLOBOCAN 2020, there were 19292789 new cases of cancer and 9958133 cancer-related deaths worldwide in 2020 [2]. The second leading cause of mortality worldwide is cancer, which accounts for 70% of fatalities in low- and middle-income nations [3].

Nanoparticles are particles with a size range of 1–100 nm. Materials with nanoscale have unique, new, and superior physical and chemical features compared to their bulk structure because of the increase in surface area per volume of the material/particle ratio [4]. Metal nanoparticles are vastly used as nanoparticle materials because they are easily synthesized. Additionally, these metal nanoparticles have been utilized frequently as novel anti-cancer medicines because of their cytotoxicity, functionality, and compatibility. Metallic nanoparticles including silver (Ag) and iron (Fe) attracted scientific community attention because of their varied industrial applications [5–7]. These products are synthesized by different biological, chemical, and physical methods. Some of these methods use toxic chemicals which can lead to harmful biological products.

WHO resources approved that approximately 80% of the world's population rely on medicinal plants as a primary source of healthcare [8]. Natural products

Beyatli Ahmet – Assistant Professor of the Department of medicinal and aromatic plants, e-mail: ahmet.beyatli@sbu.edu.tr
Shawuti Shalima – Postdoctoral fellow of the Department of Physiology, e-mail: shalima.shawuti@istanbul.edu.tr
Kariper İshak Afşin – Associate Professor of the Faculty of Education, e-mail: akariper@erciyes.edu.tr
Korkut Isık Neslişah – Graduate Student of the Department of Physiology, e-mail: naslihankorkut@gmail.com
Aktaş Zerrin – Professor of the Department of Medical Microbiology, e-mail: zaktas@istanbul.edu.tr
Serap Erdem Kuruca – Professor of the Department of Physiology, e-mail: sererdem@yahoo.com

[*] Corresponding author.

specially derived from plants play a vital role in cancer combating. More than 60% of the nowadays used anticancer agents came from plant origin [9]. Green synthesis methods involve synthesizing nanoparticles using different sources of natural products which can be plants or microorganisms [10]. Green synthesis products have low prices, are simple to produce in big quantities, and have eco-friendly properties, which have made them more popular than other approaches during last decade [11]. Due to the stability of nanoparticles, plant-mediated synthesis is considered the most appropriate method among green synthesis methods [12].

The genus *Rosa* contains nearly 100 species that are widely distributed in Europe, Asia, North America, and the Middle East [13]. *Rosa canina* L. (RC), the dog rose, is a shrub reaching up to 3.5 meters in height. The flowers are simple, white or pink. It is one of the common species in Anatolia [14]. RC was used folklorically for the prevention and therapy of flu, cold and gastrointestinal ailments [15]. It was used among people in Turkey against constipation and diabetes [14]. RC is a source of a varied group of useful compounds, such as phenolic acids, vitamins, tannins, flavonoids, triterpenes, minerals, sugars, and healthy fatty acids [16, 17]. However, the content of these phytochemicals can be different depending on diverse factors, such as the variety or the geographical origin of the plant [18]. Scientific studies on RC showed different kinds of bioactivities, for instance, antioxidant, anticarcinogenic, antidiabetic, anti-inflammatory, and anti-obesity activities [15, 17, 19–21]. In this study, we used RC fruit extract to synthesize Ag and Fe nanoparticles then evaluated its anticancer and antibacterial activity.

Materials and methods

Materials. Dulbecco's modified Eagle medium (DMEM) and Fetal bovine serum (FBS) (Gibco, UK) were used in cell culture. An anhydrous $FeCl_3$ with 98% purity (Merck, Germany), MTT [3-(4,5-dimethylthiazol-2-yl)-2,4-diphenyltetrazolium bromide] and $AgNO_3$ with 99.5% purity (Sigma-Aldrich, USA) were used as metal precursors. All reagents used were of analytical grades.

Plant Materials and Extraction. RC fruits were collected from Servetiye Village, Sakarya Province, Turkey in June 2020. The plant was authenticated by Dr. İlker Genç at Department of Pharmaceutical Botany, Faculty of Pharmacy, Istanbul University (voucher number: ISTE-117190). The shade dried fruits of RC were ground, then 10 g was suspended in 100 ml of distilled water. The mixture was stirred magnetically for 20 minutes at 60 °C, then allowed to cool at room temperature and then filtered through a Whatman no. 42 filter paper and centrifuged at 2000 rpm for 20 minutes [22]. The extract was stored at 4 °C for further use.

Phytochemicals Screening. The preliminary qualitative screening of different phytochemicals for RC fruit extract has been carried out on the aqueous extract and on the powdered specimen using standard procedures as described by the Tyler [23] and Harborne [24] methods. Results were qualitatively showed as positive (+) or negative (−).

Biosynthesis of Silver (RC-AgNPs) and Iron (RC-FeNPs) Nanoparticles. 2.5 mL from the extract solution was mixed with 1mM $AgNO_3$ in 47.5 mL deionized water and a 50 mL solution was obtained. The pH values were measured just after mixing with $AgNO_3$ metal source and after 24 hours (Table 1). The pH of the prepared $AgNO_3$ solution was 5.46 at the beginning. Then the solutions were sonicated (50 Hz, Soniclean) for 10 seconds and filtered through 200 nm filter. A similar sample preparation step was followed for iron oxide nanoparticles. 5 mL from the extract solution was taken and mixed with 0.2M $FeCl_3$ in 45 mL deionized water and a solution of 50 mL in amount was obtained. The pH values were also measured just after mixing with $FeCl_3$ and after 24 hours (Table 1). The pH of the prepared $FeCl_3$ solution was 2.20. Then the solutions were sonicated for 10 seconds and filtered through 200 nm filter.

Characterization of RC-AgNPs and RC-FeNPs. The synthesized nanoparticles were characterized through UV-Vis spectrophotometer Shimadzu 2600. The reduction of nanoparticles was monitored by UV-spectrophotometer range of absorbance from 250–480 nm at room temperature. The crystalline structures of the green-synthesized RC-AgNP) and (RC-FeNP) were examined by XRD Rigaku Flex 600 (600 models, with λ=1.5406 with a step size of 0.02 Å) at speed of 3° min^{-1}. Particle size and zeta potential were measured by Malvern Nano ZS. For SEM analysis, an aqueous suspension of RC-AgNPs and RC-FeNPs was drop-cast on a clean silicon wafer attached with carbon tape and kept it for air-drying and observed under a High-resolution scanning electron microscope (SEM Carl Zeiss ULTRA PLUS GEMINI FESEM) were used to investigate 2D surface morphologies. The composition analyses of the samples were performed by EDX (EDX spectrometer attached to SEM). Fourier transformed IR (FTIR) analyses were carried out on liquid samples with BRUKER ALPHA FTIR spectrometer in the range from 4000–500 cm^{-1}. The device had a DTGS detector, and 10 scans were conducted for each spectrum with resolution.

Cytotoxicity Assay. AGS (human gastric adenocarcinoma) cell line and HUVEC (Human umbilical vein endothelial cells) cell line was obtained from American Type Culture Collection (ATCC). Cells were cultured in DMEM with 10% FBS and 1% penicillin/streptomycin in a 5% CO_2 humidified incubator, maintained at 37 °C. The sterilized RC-AgNPs and RC-FeNPs concentrations were prepared with different dilutions with DMEM (Table 2). These different concentrations are useful in the evaluation of the manner of activity while in dose dependent or different way. Cell viability, proliferation, and activation are all measured using the colorimetric test MTT, which is sensitive, accurate, and trustworthy. The test relies on mitochondrial dehydrogenase enzymes' ability to convert the yellow, water-soluble substrate 3-(4,5-dimethylthiazol-2-yl)-2,5-diphenyl tetrazolium bromide (MTT) into a dark blue, water-insoluble formazan product. MTT assays were performed in 96-well plates. AGS cells (about 10^5cells per well) were seeded with different concentrations of RC and incubated for 72 hours. Then, supernatants were removed, and 10 µl (MTT – 5mg/mL) solution was added to each well. Following incubation at 37 °C for 3.5 h and kept dark in a humidified atmosphere at 5% CO_2 in the air. Subsequently, the supernatant was discarded, and the precipitated formazan was dissolved in dimethyl sulfoxide (100 µL per well). and the optical density of the solution was evaluated using a microplate spectrophotometer at a wavelength of 570 nm [25]. Cell viability and IC_{50} values were determined using GraphPad Prism software.

Table 1. The pH values of the RC-AgNPs and RC-FeNPs. The pH value of the RC extract was also reported for comparison

Name	0 hour	24 hour
RC	6.07	6.07
(RC-AgNPs)	6.29	5.46
(RC-FeNPs)	2.31	2.20

Table 2. RC-AgNPs and RC-FeNPs dilutions used in cytotoxicity tests

Dilutions	RC (mg/ml) – Ag (uM/ml)	RC (mg/ml) – Fe (M/ml)
1	5+20	10+0.001
1/2	2.5+10	5+0.0005
1/5	1+4	2+0.0002
1/10	0.5+2	1+0.0001

Antibacterial Activity. The antibacterial potential of RC-AgNPs and RC-FeNPs was diagnosed against total 14 different human pathogenic bacteria including three Gram-negative bacteria (Escherichia coli ATCC 35218, clinical isolates of carbapenem-resistant Klebsiella pneumoniae (CRKpn) and carbapenem-resistant Escherichia coli (CREc)) and 11 Gram-positive bacteria (Staphylococcus aureus ATCC 29213 and ATCC 25923, inducible clindamycin resistant Staphylococcus aureus (ICRSa) BAA976-1, hetero resistant Staphylococcus aureus (hVISA), clinical isolates of methicillin resistant Staphylococcus aureus (MRSA), 2 species from methicillin resistant coagulase-negative staphylococci (MR-CoNS), Vancomycin resistant Enterococcus faecium (VREf), Enterococcus faecalis ATCC 29212 and 51279, and Vancomycin susceptible Enterococcus faecalis (VSEf). The species were identified by using the Vitek 2 system (bioMerieux Vitek Inc.). Antibacterial activity was detected by minimum inhibition concentrations (MICs) which determined by the microdilution method (MIC range: 2.5–0.0012 mg/l for RC and 20 mM – 0.00976 for $AgNO_3$) by using the Clinical and Laboratory Standards Institute [26]. Briefly, 100 µl of each concentration were added to well (96-well microplate) containing 100 µl of Mueller Hinton Broth (MHB) and 10 µl of inoculum (0.5 McFarland; 1.5×10^8 colony forming units/ml). Plates were then incubated at 37 °C for 24 h. The MIC concentration of $AgNO_3$, RC and nanocapsulated extracts of synthesized Ag/RCNPs were defined as the lowest concentration inhibiting visible growth of bacteria after overnight incubation of cultures at 37 °C.

Results and Discussion

Qualitative phytochemical analysis of RC fruit extract showed the presence of different active components in the aqueous extracts (Table 3). Earlier reports of RC revealed suggest the presence of phenolic compounds (tannins, flavonoids, lignins), triterpenoids, and phytosterols [27, 28]. The existence of these constituents can be the main reason behind the biological activity.

After 24 hours of reaction, the reaction solution color changes from light to dark color, which can be seen in Figure 1 the reduction of Fe^{3+} ions it exhibits the dark color due to the excitation of Surface Plasmon vibration in a metal nanoparticle. For the reduction of Ag^+ ions, the solution color changes from light pink to light yellow.

Table 3. Preliminary phytochemical screening of RC fruit extract. Key: (−) Absent, (+) Present

Phytochemicals	Aqueous extract
Alkaloids	–
Flavonoids	+
Saponins	+
Terpenoids	+
Steroids	–
Tannins	+
Glycosides	–

The reduction of Ag and Fe ions in colloidal solutions was monitored by UV-Vis Spectrophotometer for the metal ions' stability. Firstly, RC extract's UV response was evaluated. The UV spectrum of RC (Fig. 2) indicated that a maximum absorption peak at 279 nm because of the π-π* transition of the aromatic C-C bonds and a weak shoulder obtained at 300 nm because of the n-π* transitions of the C=O bonds [29]. Secondly, Figure 2 also presented that the absorption spectra of RC-Ag (the green silver nanoparticles) that was synthesized using the RC fruit, had an absorbance peak at 420 nm. The peak at 420 nm corresponds to the surface Plasmon resonance of silver nanoparticles. It was also reported earlier in various literature that absorbance at around 420–430 nm for silver is a characteristic of these noble metal particles [30, 31]. Thirdly, the broad absorption peak (at 262 nm) was observed for green synthesized RC-FeNP solution. The absorbance of a peak at 262 nm was specific for iron [32]. A characteristic UV-Vis peak of RC-Fe shifted from 279 nm to 262 nm, showing the reaction happened and the formation of silver nanoparticles. This may be explained by the changes in the metal surfaces of the organic functional groups. Monalisa et al. reported that iron oxide produced by green syntheses with extract had an absorption peak at 261 at pH values of 5 [32]. Research work reported by Geinguenaud et.al, showed that successfully produced iron oxide nanoparticles with oligonucleotide (ODN) extract. In their work, uv-vis absorption peak was observed at 280 nm while suspension pH values were around 7 [33].

The crystalline structures of the green-synthesized RC-AgNPs and RC-FeNPs were examined by XRD analysis. The obtained patterns were demonstrated in Figure 3 with labeled indices. For RC-AgNPs, the silver nanoparticles are face-centered cubic (fcc) structure and crystalline in nature (Cubic crystalline structure, a=4.07100 Å) (JCPDS file no. 84-0713 and 04-0783). The obtained diffraction peaks at 2θ values of 26.50°, 36.78°, and 38.40°, respectively, were assigned to (220), (111), and (111) lattice planes. Those sets of lattice planes were identical to those reported for standard silver metal (JCPDS file no. 84-0713 and 04-0783). For RC-FeNPs, 4 main XRD peaks were observed. Peaks with 2θ values of 23.02°, 26.50°, 32.7°, and 35.42° were indexed to the (012), (120), (220), and (311) faces of iron monoclinic structure (a=9.61865 Å b=5.03554 Å c=13.75158 Å) (JCPDS file no. 96-210-8028). It is seen in RC-FeNP spectrum that the strong signals coming from Fe atoms and the signals originating from oxygen (O) and carbon (C) atoms together with these signals. It has been interpreted that these signals from oxygen (O) and carbon (C) atoms originate from drying.

For this reason, we paid attention to the ASTM (American Society for Testing and Materials) values, compound type, and crystal. Additionally, no other crystal phases were seen on the surfaces of the RC-AgNPs, according to the XRD spectra. The measurement of crystal phases on the surfaces of the RC-AgNPs is covered by this test. XRD analysis is a good approach for determining the values of compounds. As can be observed in the RC-FeNP spectrum, the signals from oxygen (O) and carbon (C) atoms coexist with the strong signals produced by Fe atoms. XRD card related information was summarized in Table 4.

The zeta potential is an indicator of surface charge potential which is an important parameter for understanding the stability of nanoparticles in aqueous suspensions. Table 5 summarized DLS measurements carried out on green synthesized nanoparticles. For the RC-FeNPs, the average particle size was 66 nm with polydispersity index: 0.560 (Derivative Count Rate (kcps): 128.61, Zeta Potential: +25.3 mV). On the other hand, particle sizes of RC-AgNPs were found 99 nm size with relatively homogenous distribution (polydispersity index: 0.266, Derivative Count Rate (kcps): 864.78, Zeta Potential: +8.3 mV). Both synthesized RC- FeNPs as Cosgrove [34] mentioned and AgNPs in agreement with the conclusions of Sun and colleagues [35] were stable when stored at room temperature. No aggregation of the colloidal was observed for several months. It was also observed that produced NPs had positively charged on their surface with zeta potential values of 25.3 and 8.3 respectively.

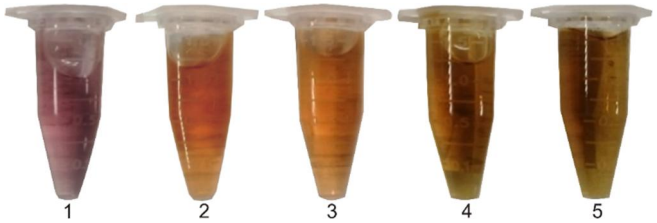

Fig. 1. Synthesis of Ag and Fe nanoparticles exhibit color change. (1) RC, (2) RC-AgNP, (3) RC-AgNP after 24 h, (4) RC-FeNP, (5) RC-FeNP after 24 h

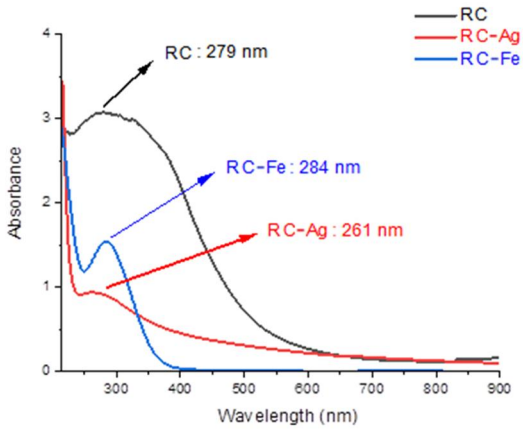

Fig. 2. UV-Visible spectrum of RC-AgNP and RC-FeNP solutions

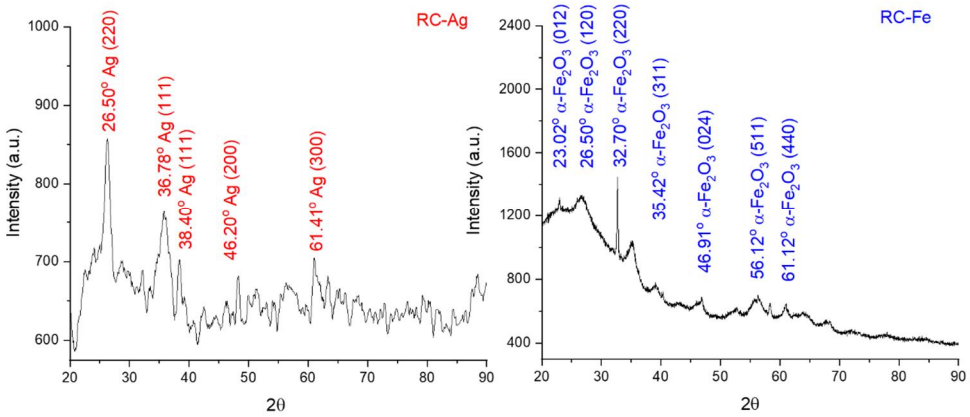

Fig. 3. X-ray powder diffractometers of RC-AgNP and RC-FeNP powders

Table 4. Observed and ASTM 2 (American Society for Testing and Materials) values, type of compound, and crystal structures

PDF Card No	ASTM Value (°)	Observed Value (°)	Compound	Crystal Structure
RC Fe				
96-210-8028	24.14	23.02	α-Fe_2O_3	Monoclinic
96-210-8028	24.21	26.50	α-Fe_2O_3	Monoclinic
96-210-8028	33.15	32.70	α-Fe_2O_3	Monoclinic
96-210-8028	35.63	35.42	α-Fe_2O_3	Monoclinic
96-210-8028	43.62	46.91	α-Fe_2O_3	Monoclinic
96-210-8028	56.15	56.12	α-Fe_2O_3	Monoclinic
96-210-8028	62.42	61.12	α-Fe_2O_3	Monoclinic
RC Ag				
04-0783	27.80	26.50	Ag	Cubic
84-0713	35.67	36.78	Ag	Cubic
04-0783	38.24	38.40	Ag	Cubic
84-0713	44.52	46.20	Ag	Cubic
84-0713	61.65	61.41	Ag	Cubic

Scanning electron microscopy (SEM) technique was used to identify the morphology and size of the green synthesized RC-FeNPs and RC-AgNPs. Figure 4 represents the surface morphology microscopy images, DLS size distribution, and EDX spectrum of green synthesized nanoparticles. The elemental composition of powdered RC-FeNPs was determined by using SEM equipped with an EDX detector. For RC-Fe, the nanoparticles appear as aggregated and spread uniform shapes. Iron nanoparticles seem also spherical with 70 nm average diameters. The EDX analysis showed the presence of iron, oxygen, silicon and chloride as seen in Figure 4 (e). Whereas silver

nanoparticles seem also with 100 nm average diameters which were furtherly confirmed by DLS size analyzer results. EDX analysis for RC-Ag showed the presence of silver, silicon and oxygen as seen in Figure 4 (f). Our findings for RC-FeNPs were in accordance with those of Önal et al., 2017 [36]. While for RC-AgNPs agreed with those of Yassin et al., 2022 [37]. In plants, chloride (Cl^-) ions are widely present and serve a vital role in photosynthesis and maintaining general homeostasis [38]. According to research, many components found by EDX analysis, such Si and Cl, were all indicated to serve as capping agents for the biogenic nanoparticles [39].

FTIR spectra of RC and RCNPs were presented in Figure 5. The absorption band at 3302 cm^{-1} was mainly attributed to OH vibration, whereas the absorption peak at 2850 cm^{-1} belonged to aliphatic symmetric vibration of CH. The absorption peaks were assigned to stretching vibration of C=C (1632 cm^{-1}), the twist of OH (1410 cm^{-1}) and stretching vibration of C-O (1318 cm^{-1}). Finally, the band in 1002 cm^{-1} belongs to the vibration peak of anhydrous CO-O-CO and stretch vibration of -CH (630 cm^{-1}) was observed. Compared to RC extract's FTIR, the disappearance of the most functional group is due to the successful reduction of metal ions. 3 main bands were demonstrated in FTIR spectrum of both RC-FeNPs and RC-AgNPs The presence of OH bonds and C=O functional groups on the RC-AgNP and RC-AgNPs were presented at a wavenumber of 3244 cm^{-1} and 1633 cm^{-1} respectively. It was reported in the literature that FeNPs exhibit a characteristic stretching Fe-O vibration peak at 621 cm^{-1} [40]. For RC-Ag NPs, stretching vibrations at 631 cm^{-1} also can be attributed to the reduction of Ag^+ to Ag. In similar green synthesis studies also reported observation of reduction of Ag^+ to Ag peak at around 585 cm^{-1} [41].

Table 5. Average diameters, polydispersity indexes, and zeta potential values of the RC-NPs

Formulation	Average Diameter (nm±SD)	PDI	ZP (mV±SD)	Derivative count rate (kcps)
RC-FeNPs	66	0.560	+25.3	128.61
RC-AgNPS	99	0.266	+8.3	864.78

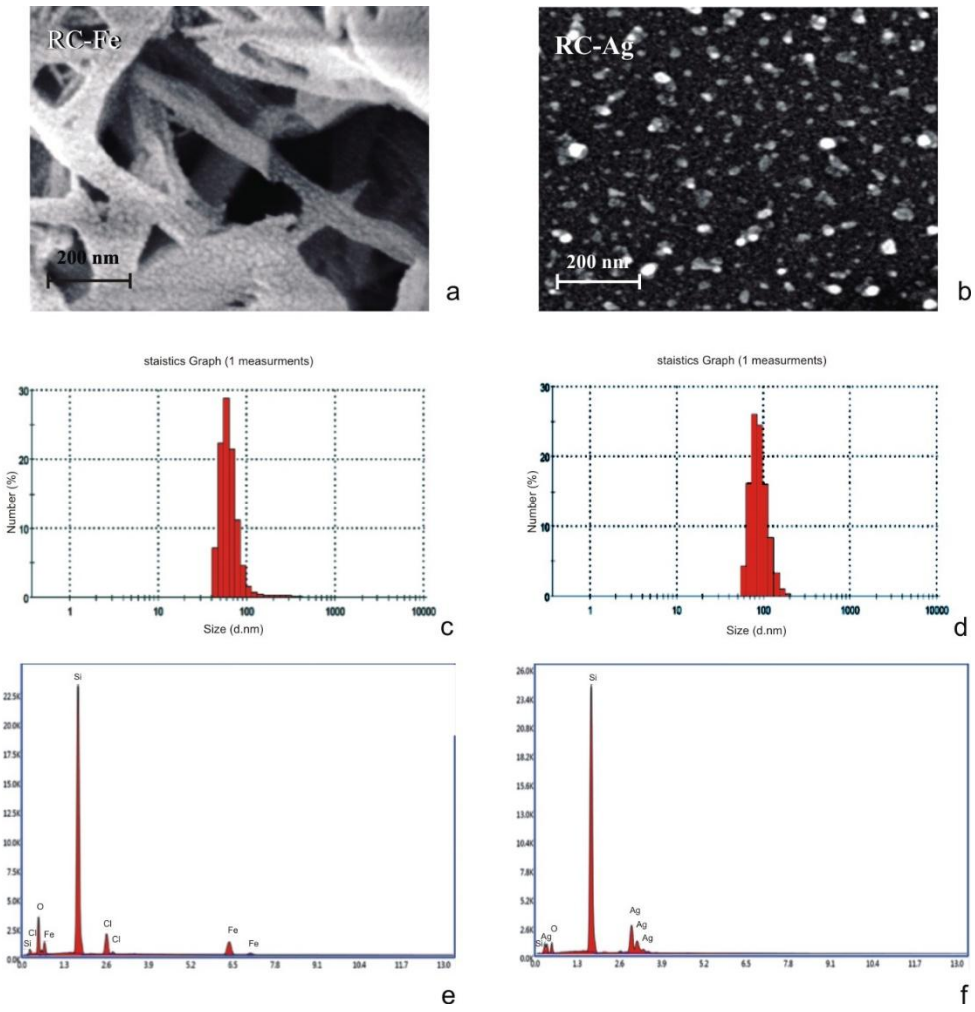

Fig. 4. SEM micrographs, DLS size distribution, and EDX of RC-FeNPs (a, c, e) and RC-AgNPs (b, d, f)

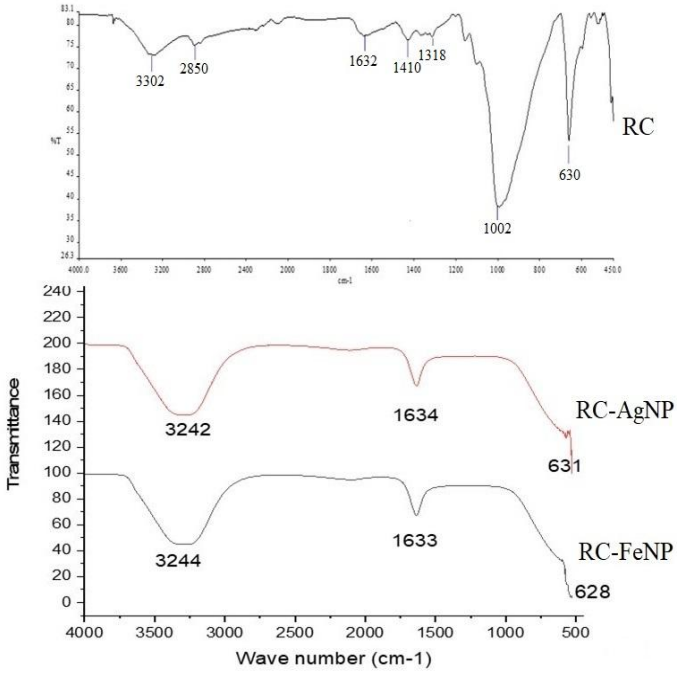

Fig. 5. FTIR spectrum of RC, RC-AgNP and RC-FeNP

Cytotoxic activity of synthesized RC-AgNP and RC-FeNP against AGS and HUVEC cell lines using MTT assay was presented in figure 6. RC-AgNP has cytotoxic effect on AGS cells in low concentrations. The results showed that diluted forms of nanoparticles are effective on AGS cell lines. For AGS cell line the cytotoxicity of RC-AgNP was noteworthy higher (1/10) in comparsion with RC-FeNP (1/2). HUVECs were used in this research as a control group. Dilution 1 of RC-AgNP has a cytotoxic effect on HUVEC cell line but its diluted forms which showed cytotoxicity on AGS cell line do not affect HUVECs. For RC-FeNP all dilutions were toxic against HUVEC cell line.

The RC extract demonstrated poor antibacterial activity in (1/2) concentration (>2.5 µg/mL), whereas (>1/3968) dilution rates of $AgNO_3$ were <0.00976 µg/mL and RC-AgNPs demonstrated antibacterial activity, MIC values ranging from 0.0390/0.3125 to 0.3125/2.5 µg/mL against the tested bacteria (Table 6). The result of RC-FeNP was not given because the results were not effective.

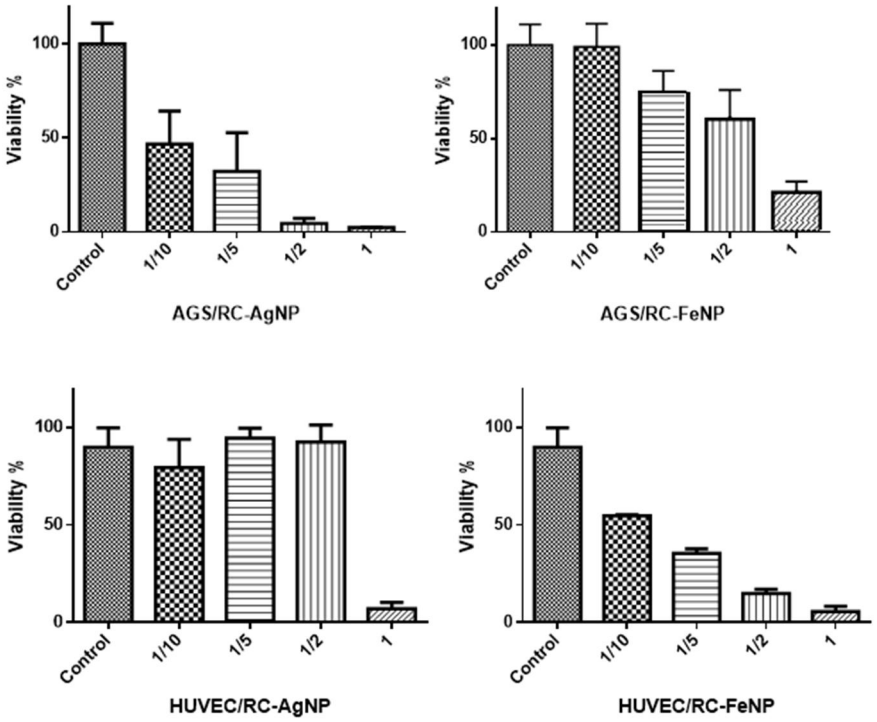

Fig. 6. Cytotoxic activity of synthesized RC-AgNP and RC-FeNP against AGS and HUVEC cell lines

The antimicrobial effects of different green synthesized silver nanoparticles against multidrug-resistant bacteria including *E. coli*, *P. aeruginosa*, and MRSA have been studied by many researchers [42–44]. In this study, our results showed that low concentration of $AgNO_3$ (<0.00976 mMol) was able to kill tested bacteria, while RC was not effective (at 2.5 mg/ml concentration) against the tested bacteria. The green synthesized RC-AgNPs were able to inhibit bacteria including multidrug pathogens. As shown in Table 6 the MIC values of RC-AgNPs against the bacteria were ranged from 0.0390/0.3125 to 0.3125/2.5 mg/mL-mMol for Gram-negative bacteria, while Gram-positive bacteria showed the MIC value of ranged from 0.078125/0.625 to 0.3125/2.5. There is no significant difference observed between Gram-negative and Gram-positive bacteria including multi resistant bacteria. It is worth mentioning that MIC values are less in RC-AgNPs than that of RC in our study.

Table 6. MIC (μg/mL) values of synthesized RC-AgNP against Gram-negative and positive bacteria

No	Bacteria	RC-AgNP (2.5 mg/ml/20 mM)	Dilution rates
1	*E. coli*	0.0390/0.3125	1/124
2	CRKpn	0.31.25/2.5	1/16
3	CREc	0.3125/2.5	1/16
4	*S. aureus* (ATCC 29213)	0.3125/2.5	1/16
5	*S. aureus* (ATCC 25923)	0.3125/2.5	1/16
6	ICRSa	0.3125/2.5	1/16
7	hVISA	0.078125/0.625	1/64
8	MRSA	0.078125/0.625	1/64
9	MR-CoNS	0.3125/2.5	1/16
10	MR-CoNS	0.078125/0.625	1/64
11	VREf	0.078125/0.625	1/64
12	*E. faecalis* (ATCC 29212)	0.15625/1.25	1/32
13	*E. faecalis* (ATCC 51279)	0.3125/2.5	1/16
14	VSEf	0.078125/0.625	1/64

Abbreviations: CRKpn, clinical isolates of carbapenem-resistant *Klebsiella pneumoniae*; CREc, carbapenem-resistant *E. coli*; ICRSa, inducible clindamycin resistant *S. aureus* BAA976-1; hVISA, hetero resistant *S. aureus*; MRSA, clinical isolates of methicillin resistant *S. aureus*; MR-CoNS, methicillin resistant coagulase-negative staphylococci; VREf, Vancomycin resistant *E. faecium*; VSEf, Vancomycin susceptible *E. faecalis*.

Conclusion

Green-synthesis of silver and iron nanoparticles using *R. canina* extract preparation, their characterizations, and its anticancer activity on human stomach cancer cell line were reported systematically. The Phytochemical analysis confirms the presence of Tannins and Flavonoids. The green synthesis of silver nanoparticles was demonstrated by visual inspection and as well as performing spectral techniques (UV-VIS absorption, FT-IR spectroscopy and SEM analysis). FT-IR results proved that bioactive compounds responsible for silver bio-reduction could be proteins and flavonoids presumed to act as reducing and capping agents for the silver and iron nanoparticles. The SEM particle size for both NPs match with DLS analysis, which were around 100 nm. The green synthesized RC-AgNPs and RC-FeNPs are cytotoxic to stomach AGS cell line in low concentrations however RC-AgNPs are not cytotoxic to HUVEC cell line in same concentrations expressing selective anticancer effect. The RC-AgNPs were able to inhibit bacteria including multidrug pathogens. However, RC-FeNPs were not effective to inhibit similar bacteria.

References

1. Hejmadi M. *Introduction to cancer biology*. Ventus Publishing, Denmark, 2014.
2. Sung H., Ferlay J., Siegel R.L. et al. *CA: Cancer Journal for Clinicians*, 2021, vol. 71, pp. 209–249. DOI: 10.3322/caac.21660.
3. *WHO. Cancer, Key facts. 2018*. URL: https://www.who.int/news-room/fact-sheets/detail/cancer.
4. Cushing B.L., Kolesnichenko V.L., O'connor C.J. *Chemical Reviews*, 2004, vol. 104, pp. 3893–3946. DOI: 10.1021/cr030027b.
5. Yesilot S., Aydin C. *Eastern Journal of Medicine*, 2019, vol. 24, pp. 111–116. DOI: 10.5505/ejm.2019.66487.
6. Saleem S., Khan M.S. *Plant Physiology and Biochemistry*, 2023, vol. 194, pp. 146–160. DOI: 10.1016/j.plaphy.2022.11.013.
7. Moraes L.C., Gomes M.P., Ribeiro-Andrade R. et al. *Environmental Pollution*, 2023, vol. 327, 121483. DOI: 10.1016/j.envpol.2023.121483.

8. Bodeker G. *WHO global atlas of traditional, complementary and alternative medicine*. World Health Organization, 2005, vol. 1.
9. Juárez P. *BoneKEy Reports*, 2014, vol. 3, p. 599. DOI: 10.1038/bonekey.2014.94.
10. Mulfinger L., Solomon S.D., Bahadory M. et al. *Journal of Chemical Education*, 2007, vol. 84, p. 322. DOI: 10.1021/ed084p322.
11. Thakkar K.N., Mhatre S.S., Parikh R.Y. *Nanomedicine: Nanotechnology, Biology and Medicine*, 2010, vol. 6, pp. 257–262. DOI: 10.1016/j.nano.2009.07.002.
12. Iravani S. Green synthesis of metal nanoparticles using plants. *Green Chemistry*, 2011, vol. 13, pp. 2638–2650. DOI: 10.1039/C1GC15386B.
13. Ercisli S. *Food Chemistry*, 2007, vol. 104, pp. 1379–1384. DOI: 10.1016/j.foodchem.2007.01.053.
14. Baytop T. *Curing with plants in Turkey, in the past and today*. Nobel Medical Books, Capa, Istanbul, 1999, 299 p.
15. Wenzig E.M., Widowitz U., Kunert O. et al. *Phytomedicine*. 2008, vol. 15, pp. 826–835. DOI: 10.1016/j.phymed.2008.06.012.
16. Larsen E., Kharazmi A., Christensen L.P. et al. *Journal of Natural Products*, 2003, vol. 66, pp. 994–995. DOI: 10.1021/np0300636.
17. Demir N., Yildiz O., Alpaslan M. et al. *LWT – Food Science and Technology*, 2014, vol. 57, pp. 126–133. DOI: 10.1016/j.lwt.2013.12.038.
18. Nybom H., Werlemark G. *VI International Symposium on Rose Research and Cultivation*, 2013, pp. 137–150. DOI: 10.17660/ActaHortic.2015.1064.17.
19. Orhan D.D., Hartevioğlu A., Küpeli E. et al. *Journal of Ethnopharmacology*, 2007, vol. 112, pp. 394–400. DOI: 10.1016/j.jep.2007.03.029.
20. Barros L., Carvalho A.M., Ferreira I.C. *Food Research International*, 2011, vol. 44, pp. 2233–2236. DOI: 10.1016/j.foodres.2010.10.005.
21. Jiménez S., Gascón S., Luquin A. et al. *PloS One*, 2016, vol. 11, e0159136. DOI: 10.1371/journal.pone.0159136.
22. Byrne F.P., Jin S., Paggiola G. et al. *Sustainable Chemical Processes*, 2016, vol. 4, p. 7. DOI: 10.1186/s40508-016-0051-z.
23. Tyler V.E. *Phytomedicines in Western Europe: potential impact on herbal medicine in the United States*. ACS Publications, 1993. DOI: 10.1021/bk-1993-0534.ch003.
24. Harborne A.J. *Phytochemical methods a guide to modern techniques of plant analysis*. Springer Science & Business Media, 1998.
25. Mosmann T. *Journal of Immunological Methods*. 1983, vol. 65, pp. 55–63. DOI:10.1016/0022-1759(83)90303-4.
26. CLSI. *Performance standards for antimicrobial susceptibility testing*. Clinical and Laboratory Standards Institute, 28th ed. CLSI supplement M100, Wayne, PA (USA), 2018.
27. Cheng B.C.Y., Fu X.Q., Guo H. et al. *Pharmacological Research*, 2016, vol. 114, pp. 219–234. DOI: 10.1016/j.phrs.2016.10.029.
28. Kerasioti E., Apostolou A., Kafantaris I. et al. *Antioxidants*, 2019, vol. 8, p. 92. DOI: 10.3390/antiox8040092.
29. Hemmati S., Mehrazin L., Ghorban H. et al. *RSC Advances*, 2018, vol. 8, pp. 21020–21028. DOI: 10.1039/C8RA90053A.
30. Bharathi V., Shanthi S. *World Journal of Pharmaceutical Research*, 2017, vol. 6, pp. 1410–1417. DOI: 10.20959/wjpr20176-8456.
31. Yousaf H., Mehmood A., Ahmad K.S. et al. *Materials Science and Engineering: C*, 2020, vol. 112, 110901. DOI: 10.1016/j.msec.2020.110901.
32. Monalisa P., Nayak P.L. *International Journal of Plant, Animal and Environmental Sciences*, 2013, vol. 3, pp. 68–78.
33. Geinguenaud F., Banissi C., Carpentier A.F. et al. *Nanomaterials*, 2015, vol. 5, pp. 1588–1609. DOI: 10.3390/nano5041588.
34. Cosgrove T. *Colloid science: principles, methods and applications*. John Wiley & Sons, 2010.
35. Sun Q., Cai X., Li J. et al. *Colloids and surfaces A: Physicochemical and Engineering aspects*, 2014, vol. 444, pp. 226–231.DOI: 10.1016/j.colsurfa.2013.12.065.
36. Önal E.S., Yatkin T., Ergüt M. et al. *International Journal of Chemical Engineering and Applications*, 2017, vol. 8, pp. 327–333. DOI: 10.18178/ijcea.2017.8.5.678.
37. Yassin M.T., Mostafa A.A.F., Al-Askar A.A. et al. *Crystals*, 2022, vol. 12, p. 603. DOI: 10.3390/cryst12050603.
38. Sidorowicz A., Szymański T., Rybka J.D. *Biology*, 2021, vol. 10, p. 784. DOI: 10.3390/biology10080784.
39. Femi-Adepoju A.G., Dada A.O., Otun K.O. et al. *Heliyon*, 2019, vol. 5, e01543. DOI: 10.1016/j.heliyon.2019.e01543.
40. Perveen S., Nadeem R., ur Rehman S. et al. *Arabian Journal of Chemistry*, 2022, vol. 15, 103764. DOI: 10.1016/j.arabjc.2022.103764.
41. Suresh G., Gunasekar P.H., Kokila D. et al. *Spectrochimica Acta Part A: Molecular and Biomolecular Spectroscopy*, 2014, vol. 127, pp. 61–66. DOI: 10.1016/j.saa.2014.02.030.
42. Campo-Beleño C., Villamizar-Gallardo R.A., López-Jácome L.E. et al. *Letters in Applied Microbiology*, 2022, vol. 75, pp. 680–688. DOI: 10.1111/lam.13759.

43. Al Mashud M.A., Moinuzzaman M., Hossain M.S. et al. *Heliyon*, 2022, vol. 8, e09920. DOI: 10.1016/j.heliyon.2022.e09920.
44. Arshad H., Saleem M., Pasha U. et al. *Electronic Journal of Biotechnology*, 2022, vol. 55, pp. 55–64. DOI: 10.1016/j.ejbt.2021.11.003.

Received March 27, 2023

Revised April 28, 2023

Accepted May 23, 2023

For citing: Beyatli A., Shawuti S., Kariper İ.A., Korkut I.N., Aktaş Z., Kuruca S.E. *Khimiya Rastitel'nogo Syr'ya*, 2023, no. 4, pp. 325–334. (in Russ.). DOI: 10.14258/jcprm.20230412740.